J Nanopart Res (2011) 13:3867–3876
DOI 10.1007/s11051-011-0339-6

RESEARCH PAPER

GoldMag nanoparticles with core/shell structure: characterization and application in MR molecular imaging

Song Zhang · Liguang Zou · Dong Zhang · Xin Pang · Hua Yang · Ying Xu

Received: 13 September 2010 / Accepted: 24 February 2011 / Published online: 26 March 2011

Abstract GoldMag is a kind of bi-functional nanoparticle, composed of a gold nanoshell and an iron oxide core. GoldMag combines the antibody immobilization property of gold nanoshell with the superparamagnetic feature of the iron oxide core. Rabbit anti-mouse IgG was immobilized on the surface of GoldMag to synthesize GoldMag-IgG in a single-step process. Transmission electron microscopy, UV/Vis spectrophotometry, zeta potential analysis, dynamic light scattering, enzyme-linked immunosorbent assay, and magnetic resonance imaging (MRI) were employed to characterize the nanostructures and the spectroscopic and magnetic properties of GoldMag and GoldMag-IgG. The antibody encapsulation efficiency of GoldMag was measured as 58.7%, and the antibody loading capacity was 88 μg IgG per milligram of GoldMag. The immunoactivity of GoldMag-IgG was estimated to be 43.3% of that of the original IgG. The cytotoxicity of GoldMag was assessed by MTT assay, which showed that it has only little influence on human dermal lymphatic endothelial cells. MR imaging of different concentrations of ultrasmall superparamagnetic iron oxide, GoldMag, and GoldMag-IgG showed that 3 μg/mL of nanoparticles could significantly affect the MRI signal intensity of GRE T2*WI. The results demonstrate that GoldMag nanoparticles can be effectively conjugated with biomacromolecules and possess great potential for MR molecular imaging.

Keywords Nanoparticles · Colloidal gold · Ultrasmall superparamagnetic iron oxide · Magnetic resonance imaging · Molecular imaging · Nanomedicine

S. Zhang · L. Zou (✉) · D. Zhang · X. Pang · H. Yang
Department of Radiology, Xinqiao Hospital, Third Military Medical University, Chongqing 400037, China
e-mail: kxyjzy@yahoo.cn

Y. Xu
Base for Drug Clinical Trial, Xinqiao Hospital, Third Military Medical University, Chongqing 400037, China

Introduction

Molecular imaging enables the visualization of cellular function and the monitoring of molecular processes in living organisms. Molecular imaging differs from traditional imaging in that probes are used to help image particular targets or pathways. Many different modalities can be used for noninvasive molecular imaging. Each modality has its different applications. With high spatial resolution and tissue resolution, MRI is particularly well-suited for morphological imaging and functional imaging. MR molecular imaging is applicable to cancer staging, angiogenesis imaging, and reporter gene imaging (Zhang et al. 2009). In the field of MR

molecular imaging, a problem to be solved is to ensure that probes accumulate abundantly in the targeted tissues. In order to improve the target-oriented properties of probes, MR contrast agents should be conjugated with specific biomarkers.

Iron oxide nanoparticles, such as superparamagnetic iron oxide (SPIO) and ultrasmall SPIO, have been widely used as MR contrast agents. Micromolar iron concentrations of SPIO can offer sufficient sensitivity for T2*-weighted imaging by affecting the spin–spin relaxation time (T2) of surrounding water molecules (Perez et al. 2004). A necessary step before applying SPIO in MR molecular imaging is its surface modification to allow conjugation with different specific biomarkers. Many approaches have been developed for modifying SPIO, including coating with polymers, liposomes, or micelles, the creation of a core–shell structure, and heterodimer formation (Sun et al. 2008). A common disadvantage of these modification approaches is that many reaction processes are usually required to synthesize specific MRI probes.

The development of bi- and multi-functional nanoparticles has attracted extensive attention in recent years because of their numerous applications in the areas of nanotechnology, material science, health, and medical treatment (Wang et al. 2008). Some researchers have used gold nanoparticles as a coating agent to synthesize core/shell structured bi-functional nanoparticles (Johng et al. 2007). These nanoparticles are usually used as drug carriers, biosensors, or photothermal agents due to their unique optical, electronic, and molecular-recognition properties. However, few studies have concerned the application of Au/Fe3O4 nanoparticles in MR molecular imaging and investigation of their magnetic characteristics.

In this study, we utilized a kind of bi-functional nanoparticle, named GoldMag, which consists of a gold nanoshell and an iron oxide core. The gold nanoshell of GoldMag can provide non-covalent binding sites for the appending of biomacromolecules (Cui et al. 2005). The iron oxide core can affect MR relaxation time through its superparamagnetic property. GoldMag can be coupled with antibody through a convenient single-step process. We are interested in the dual functionality of GoldMag nanoparticles and have investigated some of their properties to assess the feasibility of their application in MR molecular imaging.

Materials and methods

Materials

GoldMag, USPIO, and a magnetic separator were provided by Shaanxi Lifegen Co., Ltd. (China). Mouse anti-human IgG, rabbit anti-mouse IgG, goat anti-rabbit IgG/HRP, 3,3,5,5-tetramethylbenzidine (TMB) liquid substrate, and TMB stop buffer were purchased from Beijing Biosynthesis Biotechnology Co., Ltd. (China). All antibodies were purified by protein affinity chromatography. 3-(4,5-Dimethylthiazol-2-yl)-2,5-diphenyltetrazolium bromide (MTT) was supplied by Genview (USA). Human dermal lymphatic endothelial cells (HDLECs) were obtained from ScienCell Research Laboratories (USA).

Synthesis of GoldMag-IgG

GoldMag-IgG was synthesized by a single-step process (Cui et al. 2005). First, 200 μg of rabbit anti-mouse IgG (hereinafter referred to as "IgG") was dissolved in 400 μL of phosphate buffer solution (PBS) (0.01 mol/L, pH 7.4). An aliquot of 100 μL of this IgG solution was used for spectrophotometric determination of its absorbance before the reaction, while the remaining 300 μL was mixed with 1 mg of GoldMag in an Eppendorf tube (1.5 mL volume) and shaken (180 rpm, 20 min) to synthesize GoldMag-IgG. After the reaction, the products were magnetically separated for 3 min by means of a magnetic separator; the precipitate was recovered, while the supernatant was collected to determine the absorbance of the IgG solution after the reaction. The precipitate was washed twice with PBS, and the respective washing solutions were collected, designated as wash1 and wash2, and their absorbances were also measured. Next, the precipitate was mixed with bovine serum albumin (BSA) (5%, 1 mL) and shaken (180 rpm, 60 min) to block the surface non-covalent binding sites of GoldMag. Finally, GoldMag-IgG was purified magnetically and re-suspended in PBS for further application.

Scheme 1 shows a schematic diagram of GoldMag-IgG. The gray forks represent IgG, the active component of the molecular probe. IgG was bound to the GoldMag nanoparticles through the surface non-covalent binding sites of the gold nanoshell (Cui et al. 2005). The conjugation was stable because of the electrostatic interaction and van der Waals force

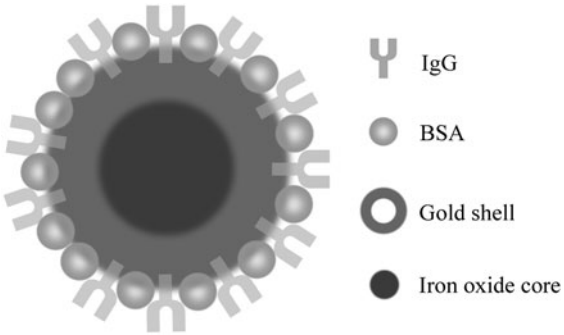

Scheme 1 Schematic diagram of GoldMag-IgG. Iron oxide core can influence MR signal intensity. Gold shell can non-covalently bind to antibody. IgG is active ingredient of molecular probe. BSA is used to block the non-specific binding sites of GoldMag surface

between GoldMag and IgG. The small gray spheres represent BSA, which was used to block the non-specific binding sites of the GoldMag surface.

Antibody encapsulation efficiency and antibody loading capacity

The absorbance at 280 nm of each solution (pre-reaction IgG, post-reaction IgG, wash1, and wash2) was determined by UV/Vis spectrophotometry (DU800, Beckman, USA) by scanning over the range 250–400 nm. The antibody encapsulation efficiency (EE, percentage of protein uptake) of GoldMag was calculated according to the following equation:

$$\mathrm{EE} = \frac{\mathrm{OD}_{280(\mathrm{pre})} - \mathrm{OD}_{280(\mathrm{post})} - \mathrm{OD}_{280(\mathrm{wash1})} - \mathrm{OD}_{280(\mathrm{wash2})}}{\mathrm{OD}_{280(\mathrm{pre})}} \times 100\% \ ,$$

where $\mathrm{OD}_{280(\mathrm{pre})}$, $\mathrm{OD}_{280(\mathrm{post})}$, $\mathrm{OD}_{280(\mathrm{wash1})}$, and $\mathrm{OD}_{280(\mathrm{wash2})}$ denote the absorbances at 280 nm of pre-reaction and post-reaction IgG solution, and the wash1 and wash2 solutions, respectively.

The antibody loading capacity (LC) of GoldMag was calculated by the following equation:

$$\mathrm{LC} = \frac{m\mathrm{Ab} \times \mathrm{EE}\%}{m\mathrm{GoldMag}},$$

where *m*Ab and *m*GoldMag denote the masses of IgG and GoldMag nanoparticles, respectively.

Properties of the nanoparticles

Aliquots (1 mL) of solutions of BSA (5%), USPIO (1 mg/mL), GoldMag (1 mg/mL), and GoldMag-IgG (1 mg/mL) were placed in a magnetic separator for 3 min to observe their magnetic responsiveness. The three types of nanoparticles were diluted with PBS (0.01 mol/L, pH 7.4). UV/Vis spectra of IgG (0.5 μg/μL), USPIO, GoldMag, and GoldMag-IgG were measured over the wavelength range 260–800 nm. The three types of nanoparticles were again diluted with PBS (0.01 mol/L, pH 7.4) to obtain the same Fe concentration of 0.1 mg/mL.

The size and morphology of USPIO, GoldMag, and GoldMag-IgG were observed by transmission electron microscopy (TEM) (Tecnai-10, Philips, Holland). The *Z*-average size (Z_{ave}) and polydispersity index (PDI) of USPIO, GoldMag, and GoldMag-IgG nanoparticles were determined by the dynamic light scattering (DLS) technique (Nano zs90, Malvern, England). The three types of nanoparticles were diluted with double distilled water (pH 6.0) to a concentration of 20 μg/mL. Solutions were placed in a transparent cup of volume 1.2 mL at 25 °C. The USPIO, GoldMag, and GoldMag-IgG nanoparticles were likewise diluted with double distilled water (pH 6.0) at 25 °C for zeta potential analysis (Nano zs90, Malvern, England).

Immunoactivity of GoldMag-IgG

To investigate the influence of GoldMag on IgG immunoactivity, a double-antibody sandwich ELISA method was performed to detect the immunoactivity of IgG before and after binding to GoldMag (Boutry et al. 2005). The working concentration of each antibody was set according to the supplier's instructions. First, 100 μL of mouse anti-human IgG (1 μg/mL) was used to coat a 96-well plate (Corning, USA) for 12 h at 4 °C. Then, the content of each well was

replaced by 100 μL of blocking BSA (1%) for 1 h at 37 °C. Subsequently, the content of each well was replaced by 100 μL of rabbit anti-mouse IgG (diluted to 1:500 with PBS) or 100 μL of GoldMag-IgG (diluted to 1:500 with PBS), respectively, to react with the mouse anti-human IgG for 1 h at 37 °C. Thereafter, the content of each well was replaced by 100 μL of goat anti-rabbit IgG/HRP (diluted to 1:1000 with PBS) to react for 1 h at 37 °C. In addition, the content of each well was replaced by 100 μL of TMB substrate to react with HRP for 15 min at room temperature. Between the various above-mentioned steps, the wells of the 96-well plate were washed three times with PBS (0.01 mol/L, pH 7.4). Finally, 100 μL of stop buffer was added to end the reaction between TMB and HRP. The absorbance of each well at 450 nm was determined by ELISA (Sunrise, Tecan, Switzerland).

Cytotoxicity of GoldMag

An MTT assay was applied to measure the cytotoxicity of GoldMag toward normal cells (Mosmann 1983). HDLECs were cultured in endothelial cell medium (ECM) (ScienCell Research Laboratories, USA). The ECM consisted of 500 mL of basal medium, 25 mL of fetal bovine serum (FBS), 5 mL of endothelial cell growth supplement (ECGS), and 5 mL of penicillin/streptomycin solution. Cells were cultured at 37 °C in a humidified atmosphere supplemented with 5% CO_2.

The HDLECs were plated at a density of approximately 3 × 103 cells per well in a 96-well plate and cultured for 24 h. The cells were exposed to a range of GoldMag concentrations (1, 5, 10, 50, 100, 500, and 1000 μg/mL in ECM) to investigate the dependence of the cytoactivity of the HDLECs on the GoldMag concentration. In order to calculate the average absorbances, each concentration was deployed in six wells. The cultures were incubated for different time periods of 24, 48, and 72 h to study the time dependence of the influence of GoldMag on the cytoactivity of the HDLECs. At the end of each incubation period, 20 μL MTT (5 μg/μL) was added to each well and the mixtures were further incubated for 4 h. The contents were then replaced with 150 μL of dimethyl sulfoxide (DMSO) to dissolve the purple-colored formazan complex formed by reduction of MTT. Finally, the absorbances at 490 nm were determined by ELISA (Sunrise, Tecan, Switzerland).

Magnetic resonance imaging

The USPIO, GoldMag, and GoldMag-IgG were diluted with double distilled water to the same Fe concentration. From left to right (Fig. 7a, b), the Fe concentration in each tube was 0, 1, 3, 5, 10, and 15 μg/mL. The Eppendorf tubes were doused in double distilled water. MR studies were performed with a 3.0 T MR imaging system (Signa HDx 3.0 T, GE, USA). The head coil was used to obtain gradient-recalled echo (GRE) T2*-weighted images. All Eppendorf tubes were examined by a GRE T2*-weighted sequence (TR = 500 ms, TE = 15, 20, 25, 30, 35, 40 ms, flip angle = 20°, FOV = 20 cm, slice thickness = 2 mm, matrix = 512 × 256, NEX = 2). R2 star software was used to calculate the GRE T2*WI signal intensity and relaxation time of each solution.

Results and discussion

The nanoshell of GoldMag has a tendency to couple with macromolecules (Thobhani et al. 2010). The oval-like shape of GoldMag provided enough binding sites for the coupling of IgG. As shown in Fig. 1, the absorbance of the pre-reaction IgG solution at 280 nm was much higher than those of the post-reaction IgG solution and the wash1 and wash2 solutions. $OD_{280(pre)}$, $OD_{280(post)}$, $OD_{280(wash1)}$, and $OD_{280(wash2)}$ were 0.921, 0.253, 0.091, and 0.036,

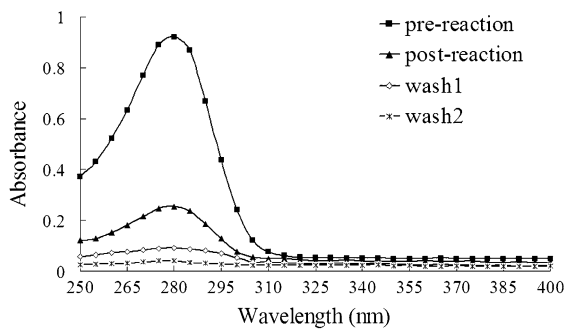

Fig. 1 Absorption curve of IgG solution. The absorption peak of each solution was significantly different at 280 nm wavelength

respectively. After conjugation of IgG and GoldMag, the absorbance of the IgG solution significantly decreased, which indicated that IgG had been successfully immobilized on the GoldMag surface. Calculated by the formulae given above, the antibody EE of GoldMag was 58.7% and the antibody LC was 88 μg IgG per milligram of GoldMag. Antibody EE and LC are both key design parameters for antibody and drug conjugation. The values of EE and LC are sensitive to many factors, including charge, hydrophobicity, and morphology (size, shape, and lamellarity) (Nicholas et al. 2000; Sun and Chiu 2005). The values of EE and LC differ among studies. Shah and Amiji (2006) reported that the loading capacity of saquinavir on biodegradable polymeric nanoparticles was 28 μg/mg, and that the coupling efficiency was 60%. Esmaeili et al. (2008) reported that the FOL-targeted NPs had a larger size (216 ± 18 nm) with a higher DTX content (0.45 ± 0.02%), while non-targeted NPs were of size 175 ± 13 nm with a DTX content of 0.34 ± 0.01%.

The iron oxide core of GoldMag displays typical superparamagnetic character, which allows the GoldMag nanoparticles to be quickly aggregated together under the influence of an external magnetic field. USPIO, GoldMag, and GoldMag-IgG showed high magnetic responsivenesses after they were separated in a magnetic separator for 3 min (Fig. 2). UV/Vis spectra of the respective solutions were acquired over the wavelength range 260–800 nm (Fig. 3). The absorption peaks of IgG, USPIO, GoldMag, and GoldMag-IgG were located at about 280, 380, 550,

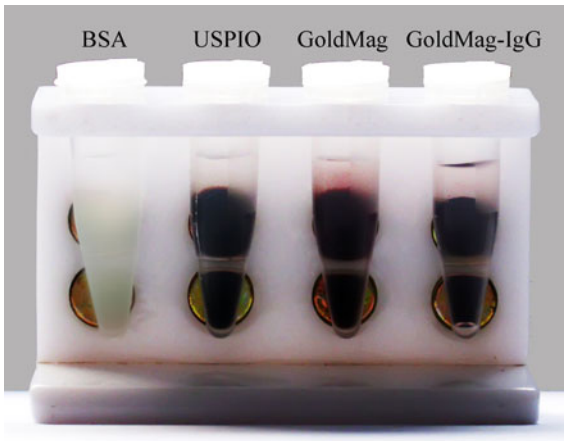

Fig. 2 Magnetic responsiveness of USPIO, GoldMag, and GoldMag-IgG solutions

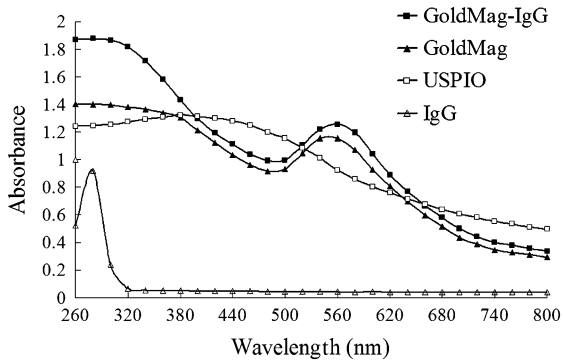

Fig. 3 Absorption curve of different solutions. The absorbance value of GoldMag-IgG was obviously higher than that of GoldMag at 280 nm

and 560 nm, respectively. Larger size of the nanoparticle results in a broader absorption spectrum and a red-shifted maximum absorption wavelength (Cui et al. 2005). Compared with GoldMag, the absorption peak of GoldMag-IgG underwent a red-shift of 10 nm and the absorption spectrum was slightly wider because of the IgG coating (Xu et al. 2007). As 280 nm is a typical absorption peak of a protein, and the spectrum of GoldMag-IgG featured an obvious absorption peak at 280 nm, it reflected the presence of IgG in the GoldMag-IgG.

The TEM results for USPIO, GoldMag, and GoldMag-IgG showed that the nanoparticles were oval-like in shape. The results of Kolmogorov–Smirnov tests for normality showed that the sizes of the nanoparticles conformed to a normal distribution. The particle sizes of USPIO, GoldMag, and GoldMag-IgG were 14.7 ± 1.4, 47.7 ± 4.1, and 67.3 ± 5.5 nm, respectively (Fig. 4). Particle size can be influenced by many factors during the synthesis process, including reaction time, temperature, substrate concentration, and pH (Yurdakal et al. 2007). It is difficult to ensure uniformity of particle size. The core of GoldMag was USPIO with a mean diameter of 14.7 nm. The thickness of the gold nanoshell was thus about 16.5 nm. After coupling with IgG, the mean diameter of GoldMag-IgG increased by 19.6 nm. The gray scale in the TEM image reflects the electron density of the nanoparticles (Ali and Mayes 2010). The electron density of IgG was lower than that of GoldMag, so it surrounded GoldMag like a thin cloud (Fig. 4c).

The DLS is a technique that is commonly used to determine the size distribution profile of small

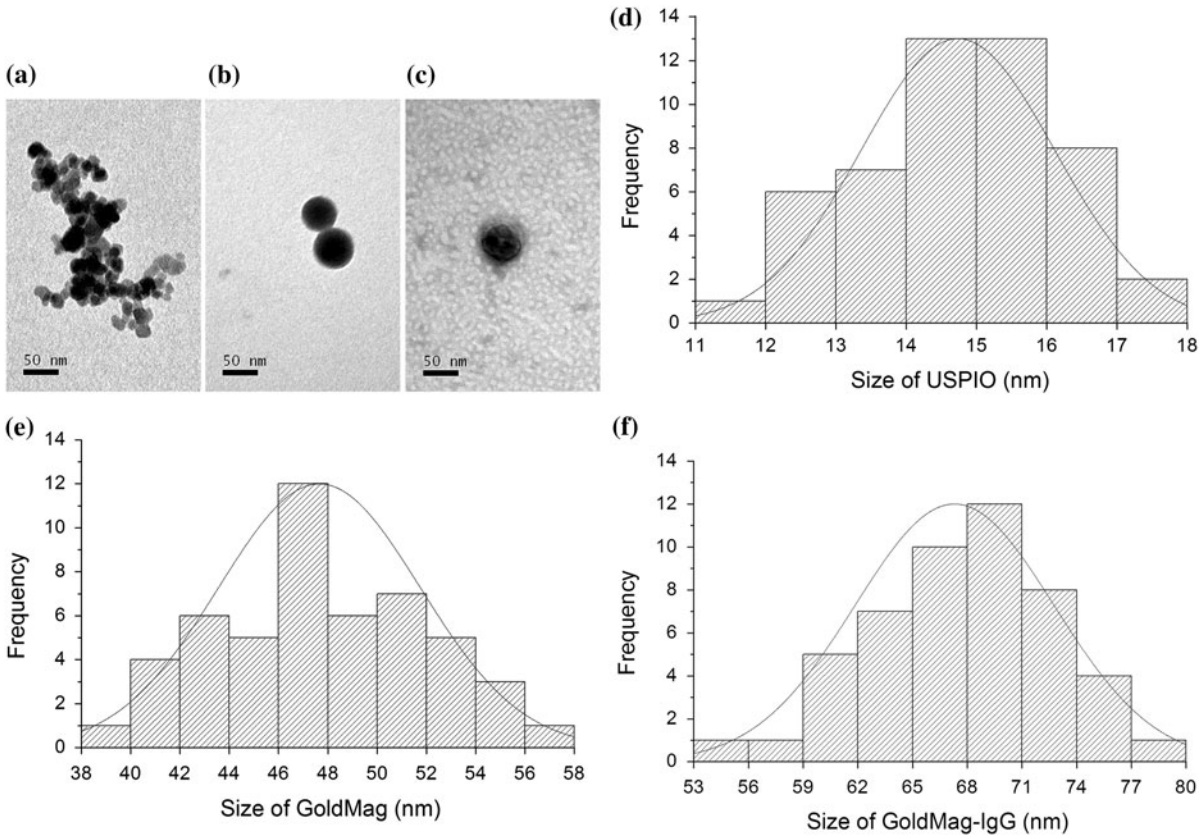

Fig. 4 TEM images of USPIO (**a**), GoldMag (**b**), and GoldMag-IgG (**c**). The size distribution histogram of USPIO (14.7 ± 1.4 nm) (**d**), GoldMag (47.7 ± 4.1 nm) (**e**), and GoldMag-IgG (67.3 ± 5.5 nm) (**f**)

particles in suspension. DLS results showed that the Z_{ave} values of USPIO, GoldMag, and GoldMag-IgG were 17.4, 49.9, and 72.5 nm, respectively (Fig. 5). The particle size of GoldMag-IgG was larger than that of GoldMag. The reason might be that the presence of IgG on the surface of GoldMag-IgG. The PDI of the USPIO, GoldMag, and GoldMag-IgG nanoparticles were 0.097, 0.071, and 0.075, respectively (Fig. 5). PDI = 0.05 is a threshold value for assessing whether nanoparticles are monodisperse in a given solvent. Generally, size distributions with a PDI of less than 0.1 are considered to be monodisperse (Gokarn et al. 2009). The higher the PDI, the more easily the nanoparticles can aggregate together. The three kinds of nanoparticles considered here displayed monodispersity in double distilled water, but also showed a tendency for aggregation. Some aggregated nanoparticles would affect the Z_{ave} results. Hence, the Z_{ave} values were larger than the TEM diameters for the three kinds of nanoparticles.

The results of zeta potential analyses showed that the potentials of USPIO, GoldMag, and GoldMag-IgG were 10.1 ± 4.1, 13.7 ± 5.6, and −16.1 ± 3.9 mV, respectively. The potentials of USPIO and GoldMag were both positive, while that of GoldMag-IgG was negative. The zeta potential is the equilibrium electric potential at the shear plane. The shear plane (an imaginary surface) is used to represent the effective location of the solid–liquid interface, where the liquid velocity is zero. The surface potential of nanoparticles can be significantly altered by changing the pH of the medium (Yu and Chow 2004). Double distilled water (pH 6.0) is a slightly acidic medium. The positive charges on GoldMag and USPIO were expected due to the tendency of the nanoparticle surfaces to absorb H^+ in an acidic environment. The negative charge of IgG resulted in a net negative charge on GoldMag-IgG (Liang et al. 2007). Surface charge plays an important role during endocytosis. The endocytosis index in vitro is minimal when the zeta potential is close to

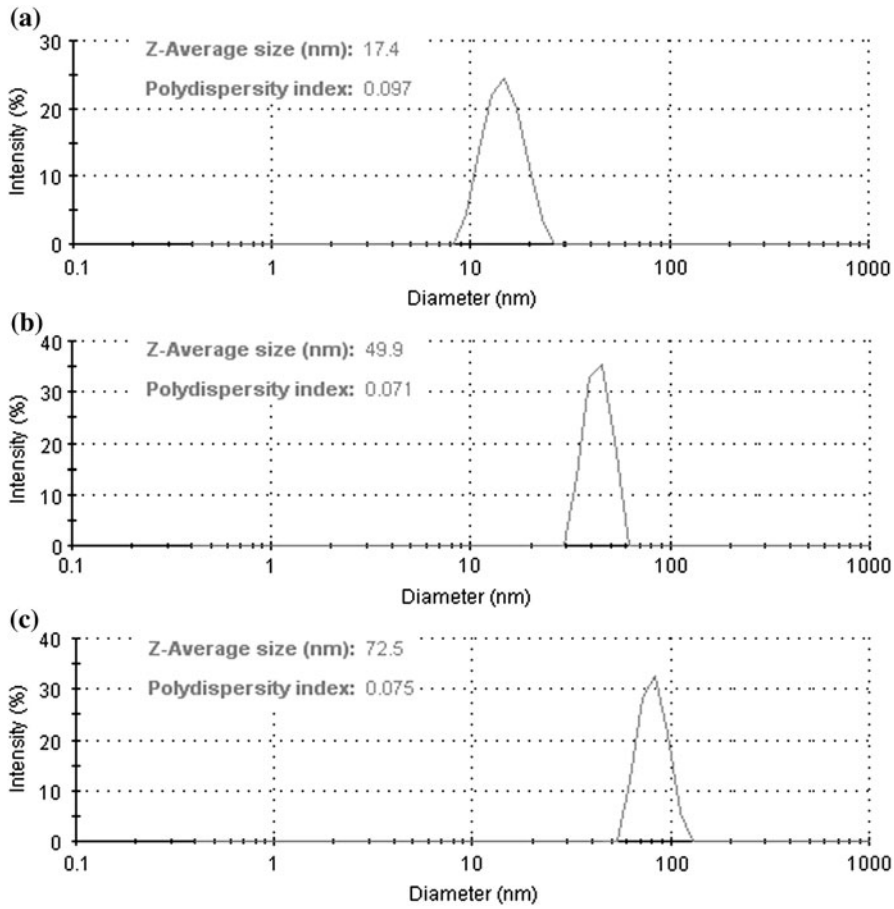

Fig. 5 DLS results of USPIO (**a**), GoldMag (**b**), and GoldMag-IgG (**c**)

zero. In contrast, phagocytosis is increased with a higher surface charge, irrespective of whether the charge is negative or positive (Neuberger et al. 2005).

Following the ELISA steps mentioned above, the absorbance of IgG was measured as 0.879. After reaction with one equivalent of GoldMag, the absorbance of GoldMag-IgG was measured as 0.381. The immunoactivity percentage of GoldMag-IgG was defined as the ratio of GoldMag-IgG immunoactivity to that of IgG. The immunoactivity of GoldMag-IgG was thus reduced to 43.3% of that of the original IgG. This ELISA result showed that GoldMag-IgG retained a certain level of the immunoactivity of IgG. From this, we conclude that GoldMag-IgG has some potential to be used as a molecular probe for in vitro and in vivo experiments. Among various antibody labeling methods, both immune and chemical conjugation reduce antibody immunoactivity and enzymatic activity (Bosman et al. 1983). The conjugation of GoldMag and IgG was induced by electrostatic interaction and van der Waals forces, and so can be classified as physical conjugation. The reduction of IgG immunoactivity may be due to various reasons. However, it is known that excess antibody coating can lead to inferior performance of conjugates due to effects such as steric hindrance, antibody orientation, and the formation of multiple protein layers (Thobhani et al. 2010).

The cytotoxicity of GoldMag toward HDLECs was assessed by MTT assay. HDLECs were cultivated with GoldMag solutions of different concentrations for different time periods (24, 48, and 72 h). GoldMag can be encapsulated by HDLECs through endocytosis, and then decomposed by enzymes within the cells (Sung et al. 2009). The solutions of GoldMag had only a slight cytotoxic effect on the HDLECs, but the influence of GoldMag on the cytoactivity of the HDLECs was increased with increasing GoldMag concentration and extension of the cultivation time (Fig. 6). The general variation trends in the absorbances over the different

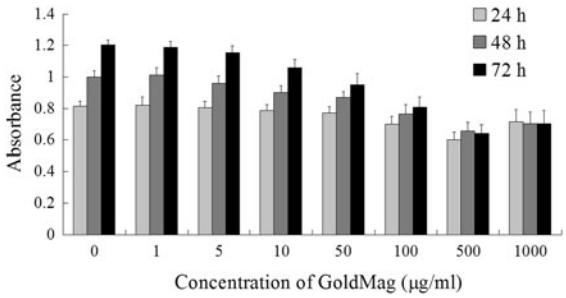

Fig. 6 Cytotoxicity of GoldMag on normal HDLECs assessed by MTT assay

time periods were similar (24, 48, and 72 h). At a GoldMag concentration of ≤100 μg/mL, the cytoactivity of HDLECs was not significantly influenced and the HDLECs continued to proliferate with extension of the cultivation time. At a GoldMag concentration of >100 μg/mL, the HDLECs no longer proliferated with extension of the cultivation time. In the process of washing of the GoldMag nanoparticles, it was difficult to remove all nanoparticles from each well; some nanoparticles remain adhered to the wall and bottom of the 96-well plate. As GoldMag nanoparticles are red, a higher concentration of GoldMag would result in a higher absorbance in MTT assay. So, the absorbances of each well increased at the 500 and 1000 μg/mL concentrations of GoldMag, even though the number of cells in each well decreased.

The spin-echo sequence is the most commonly used MRI pulse sequence, and only the "true" T2 relaxation can be seen with this sequence. The transverse relaxation in GRE sequence is a combination of "true" T2 relaxation and the relaxation caused by magnetic field inhomogeneity (Chavhan et al. 2009). The GRE sequence is commonly used to depict hemorrhage, calcification, and iron deposition in various tissues and lesions. The iron oxide core of GoldMag would result in magnetic field inhomogeneity by shortening the spin–spin relaxation times (T2) of surrounding protons, which allows GoldMag to be used as a T2* contrast agent. Gradually increasing concentrations of USPIO, GoldMag, and GoldMag-IgG nanoparticles were used for MR GRE T2*-weighted imaging. At a GoldMag concentration of 3 μg/mL, the decreasing of MRI signal intensity (Fig. 7a) and relaxation time (Fig. 7b) can be detected. With increasing Fe concentration, the MRI

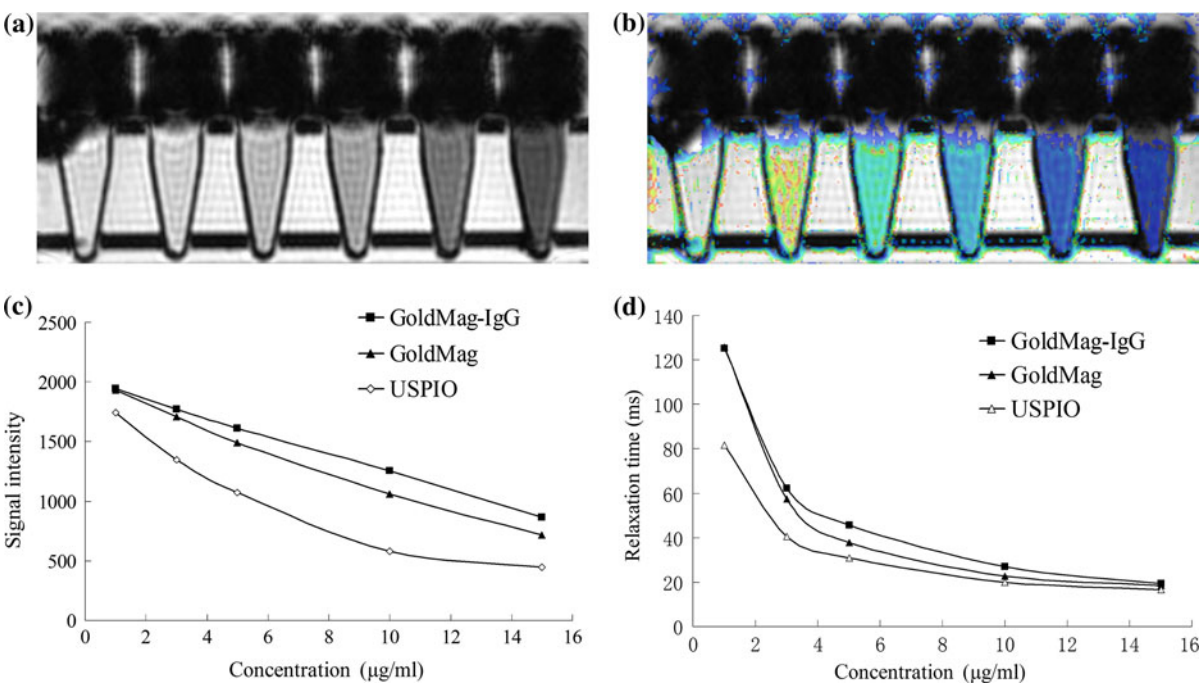

Fig. 7 MRI images of different Fe concentrations of nanoparticle solutions. **a** and **b** represent signal intensity and relaxation time of GoldMag solution respectively. **c** and **d** represent the correlation of nanoparticle concentrations with MR signal intensity and relaxation time, respectively

signal intensity and relaxation time of GoldMag solution decreased significantly. Besides, the superparamagnetic properties of USPIO, GoldMag, and GoldMag-IgG were compared by GRE T2*-weighted imaging at the same Fe concentration. For the three kinds of nanoparticles, the general variation trends in the GRE T2*WI signal intensity (Fig. 7c) and relaxation time (Fig. 7d) were similar. However, the signal intensity and relaxation time of GoldMag were relatively higher than those of USPIO. A layer of gold is wrapped around the iron oxide core of GoldMag, which results in the separation of iron oxide and water. As a result, the shortening effect of iron oxide on the spin–spin relaxation time (T2) of water is weakened. Moreover, the superparamagnetic property of GoldMag-IgG is further weakened by the layer of IgG.

One promising approach for increasing SPIO accumulation in diseased tissues and lesions, referred to as active targeting or specific targeting, involves conjugating target agents on the surface of SPIO (Thorek et al. 2006). Via a polymer coating, the SPIO usually bears some active groups, such as amines, sulfhydryls, carboxyls, etc., which subsequently allow for more controllable conjugations. Active targeting has more advantages than passive targeting since it not only provides physiological information but also offers insight into specific molecular mechanisms (Thorek et al. 2006). The main obstacle to synthesize highly sensitive molecular probes has been the complex reaction steps required. GoldMag can be coupled with antibody through a single-step process, which reduces the number of steps of the synthesis process. The synthesis process is convenient, requiring only about 100 min. In addition, GoldMag-IgG nanoparticles are small enough to leak out of the vascular bed and diffuse into the extracellular space. GoldMag-IgG maintains a certain binding affinity of the antibody, which subsequently guides the molecular probe to the target tissue.

As a hyperthermal agent, a commendable property of colloidal gold is that it displays excellent therapeutic features. Gold nanoparticles strongly absorb near-infrared (NIR) radiation and can then transfer this energy to the surrounding environment as heat, which ultimately results in cell death (Jiang et al. 2009). Among various kinds of photothermal ablation technologies, NIR absorption photothermal therapy is particularly advantageous because it is relatively harmless to normal tissues (Norman et al. 2008; Wang et al. 2009). So, GoldMag nanoparticles also have great potential in the field of NIR photothermal therapy.

Although GoldMag possesses many of the advantages of bi-functional nanoparticles, its further development is still required. If GoldMag nanoparticles were to be injected intravenously, they would immediately interact with plasma proteins due to their lack of a surface polymer coating. This would result in a short residence time of GoldMag in the circulatory system. Only a small proportion of the GoldMag nanoparticles would reach the target tissue, with the remainder being non-specifically accumulated in macrophages. Nevertheless, some parameters, including the size, charge, and hydrophobicity of the nanoparticles, may be optimized so that more GoldMag is directed toward the target tissue (Jiang et al. 2009).

Conclusions

GoldMag nanoparticles are composed of a gold nanoshell and an iron oxide core. The gold nanoshell can immobilize antibodies on the GoldMag surface, while the iron oxide core possesses superparamagnetic properties. In this study, we have introduced a single-step synthesis method for immobilizing IgG on the GoldMag surface. The results demonstrated that IgG was stably coupled with GoldMag. GoldMag-IgG retained 43.3% of the immunoactivity of the original IgG. A small amount of GoldMag can effectively reduce MRI signal intensity and relaxation time, while having only a slight cytotoxic effect on HDLECs. Therefore, GoldMag nanoparticles might be used as a paramagnetic medium to synthesize specific probes for MR molecular imaging.

Acknowledgments The authors would like to express thanks to Prof. Wei Sun for reviewing the manuscript. The study was financed by the National Natural Science Foundation of China (Grant Nos. 30770609, 81071197).

References

Ali AMI, Mayes AG (2010) Preparation of polymeric core–shell and multilayer nanoparticles: surface-initiated polymerization using in situ synthesized photoiniferters. Macromolecules 43:837–844. doi:10.1021/ma9019812

Bosman FT, Cramer-Knijnenburg G, Van Bergen Henegouw J (1983) Efficiency and sensitivity of indirect immunoperoxidase methods. Histochem Cell Biol 77:185–194. doi:10.1007/BF00506561

Boutry S, Burtea C, Laurent S, Toubeau G, Elst LV, Muller RN (2005) Magnetic resonance imaging of inflammation with a specific selectin-targeted contrast agent. Magn Reson Med 53:800–807. doi:10.1002/mrm.20403

Chavhan GB, Babyn PS, Thomas B, Shroff MM, Haacke EM (2009) Principles, techniques, and applications of T2*-based MR imaging and its special applications. Radiographics 29:1433–1449. doi:10.1148/rg.295095034

Cui YL, Wang YN, Hui WL, Zhang ZF, Xin XF, Chen C (2005) The synthesis of GoldMag nano-particles and their application for antibody immobilization. Biomed Microdevices 7:153–156. doi:10.1007/s10544-005-1596-x

Esmaeili F, Ghahremani MH, Ostad SN, Atyabi F, Seyedabadi M, Malekshahi MR, Mohsen Amini, Dinarvand R (2008) Folate-receptor-targeted delivery of docetaxel nanoparticles prepared by PLGA–PEG–folate conjugate. J Drug Target 16:415–423. doi:10.1080/10611860802088630

Gokarn YR, Fesinmeyer RM, Saluja A, Cao S, Dankberg J, Goetze A, Remmele RL, Narhi LO, Brems DN (2009) Ion-specific modulation of protein interactions: anion-induced, reversible oligomerization of a fusion protein. Protein Sci 18:169–179. doi:10.1002/pro.20

Jiang JK, Oberdorster G, Biswas P (2009) Characterization of size, surface charge, and agglomeration state of nanoparticle dispersions for toxicological studies. J Nanopart Res 11:77–89. doi:10.1007/s11051-008-9446-4

Johng HM, Yoo JS, Yoon TJ, Shin HS, Lee BC, Lee C, Lee JK, Soh KS (2007) Use of magnetic nanoparticles to visualize threadlike structures inside lymphatic vessels of rats. Evid-based Compl Alt 4:77–82. doi:10.1093/ecam/nel057

Liang ZH, Wu JX, Huang JL, Tan WP, Ke ML, Liu RY, Huang BJ, Xiao X, Zhao P, Huang WL (2007) Bioactivity and stability analysis of endostatin purified from fermentation supernatant of 293 cells transfected with Ad/rhEndo. Protein Expr Purif 56:205–211. doi:10.1016/j.pep.2007.08.008

Mosmann T (1983) Rapid colorimetric assay for cellular growth and survival: application to proliferation and cytotoxicity assays. J Immunol Methods 65:55–63. doi:10.1016/0022-1759(83)90303-4

Neuberger T, Schopf B, Hofmann H, Hofmann M, Rechenberg BV (2005) Superparamagnetic nanoparticles for biomedical applications: possibilities and limitations of a new drug delivery system. J Magn Magn Mater 293:483–496. doi:10.1016/j.jmmm.2005.01.064

Nicholas AR, Scott MJ, Kennedy NI, Jones MN (2000) Effect of grafted polyethylene glycol (PEG) on the size, encapsulation efficiency and permeability of vesicles. Biochim Biophys Acta 1463:167–178. doi:10.1016/S0005-2736(99)00192-3

Norman RS, Stone JW, Gole A, Murphy CJ, Sabo-Attwood TL (2008) Targeted photothermal lysis of the pathogenic bacteria, *Pseudomonas aeruginosa*, with gold nanorods. Nano Lett 8:302–306. doi:10.1021/nl0727056

Perez JM, Josephson L, Weissleder R (2004) Use of magnetic nanoparticles as nanosensors to probe for molecular interactions. Chembiochem 5:261–264. doi:10.1002/cbic.200300730

Shah LK, Amiji MM (2006) Intracellular delivery of saquinavir in biodegradable polymeric nanoparticles for HIV/AIDS. Pharm Res 23:2638–2645. doi:10.1007/s11095-006-9101-7

Sun BY, Chiu DT (2005) Determination of the encapsulation efficiency of individual vesicles using single-vesicle photolysis and confocal single-molecule detection. Anal Chem 77:2770–2776. doi:10.1021/ac048439n

Sun C, Lee JSH, Zhang MQ (2008) Magnetic nanoparticles in MR imaging and drug delivery. Adv Drug Deliver Rev 60:1252–1265. doi:10.1016/j.addr.2008.03.018

Sung CK, Hong KA, Lin S, Lee Y, Cha J, Lee JK, Hong CP, Han BS, Jung SI, Kim SH, Yoon KS (2009) Dual-modal nanoprobes for imaging of mesenchymal stem cell transplant by MRI and fluorescence imaging. Korean J Radiol 10:613–622. doi:10.3348/kjr.2009.10.6.613

Thobhani S, Attree S, Boyd R, Kumarswami N, Noble J, Szymanski M, Porter RA (2010) Bioconjugation and characterisation of gold colloid-labelled proteins. J Immunol Methods 356:60–69. doi:10.1016/j.jim.2010.02.007

Thorek DLJ, Chen AK, Czupryna J, Tsourkas A (2006) Superparamagnetic iron oxide nanoparticle probes for molecular imaging. Ann Biomed Eng 34:23–38. doi:10.1007/s10439-005-9002-7

Wang L, Bai J, Li Y, Huang Y (2008) Multifunctional nanoparticles displaying magnetization and near-IR asorption. Angew Chem Int Ed 47:2439–2442. doi:10.1002/anie.200800014

Wang C, Chen J, Talavage T, Irudayaraj J (2009) Gold nanorod/Fe_3O_4 nanoparticle "nano-pearl-necklaces" for simultaneous targeting, dual-mode imaging, and photothermal ablation of cancer cells. Angew Chem Int Ed 48:2759–2763. doi:10.1002/anie.200805282

Xu ZC, Hou YL, Sun SH (2007) Magnetic core/shell Fe_3O_4/Au and Fe_3O_4/Au/Ag nanoparticles with tunable plasmonic properties. J Am Chem Soc 129:8698–8699. doi:10.1021/ja073057v

Yu S, Chow GM (2004) Carboxyl group (–CO_2H) functionalized ferrimagnetic iron oxide nanoparticles for potential bioapplications. J Mater Chem 14:2781–2786. doi:10.1039/b404964k

Yurdakal S, Loddo V, Ferrer BB, Palmisano G, Augugliaro V, Farreras JG, Palmisano L (2007) Optical properties of TiO_2 suspensions: influence of pH and powder concentration on mean particle size. Ind Eng Chem Res 46:7620–7626. doi:10.1021/ie070205h

Zhang D, Feng XY, Henning TD, Wen L, Lu WY, Pan H, Wu X, Zou LG (2009) MR imaging of tumor angiogenesis using sterically stabilized Gd-DTPA liposomes targeted to CD105. Eur J Radiol 70:180–189. doi:10.1016/j.ejrad.2008.04.022